Acta Mech 210, 135–157 (2010)
DOI 10.1007/s00707-009-0188-x

Alfred Kluwick · Edward A. Cox · Alfred Exner · Christoph Grinschgl

On the internal structure of weakly nonlinear bores in laminar high Reynolds number flow

Received: 11 November 2008 / Revised: 29 April 2009 / Published online: 5 July 2009

Abstract The paper deals with the internal structure of hydraulic jumps in near-critical single-layer flows which replaces the discontinuities predicted by hydraulic theory if viscous effects acting inside a thin laminar boundary layer are properly accounted for. In the limit of large Reynolds number this leads to a structure problem formed by the classical triple-deck equations supplemented with a novel nonlinear interaction relationship which allows for the passage through the critical state. Hydraulic jumps are shown to represent eigensolutions of the structure problem where this passage is achieved by the local thickening of the boundary layer which acts as a viscous hump. The effects of detuning and dispersion due to streamline curvature and surface tension on the internal structure of hydraulic jumps are studied in detail. In addition, the interaction of hydraulic jumps with surface mounted obstacles is investigated.

1 Introduction

If the flow in a liquid layer is forced to adjust to a new downstream state a hydraulic jump or bore may form. In many cases of practical importance, including applications in civil, mechanical as well as chemical engineering, the streamwise extent of the adjustment region is small compared to a characteristic length of the global flow field. As a result the phenomenon can be treated as a jump discontinuity similar to gasdynamic shocks (e.g. [18,21,30]). In contrast to gasdynamic shocks, however, where the resulting jump conditions represent an exact solution of the governing equations if dissipative effects are neglected, the corresponding relationships for hydraulic jumps require the acceleration of the fluid in the direction normal to the solid boundary to be small and, therefore, are only approximate in this limit. Also, while the internal dissipative structure of gasdynamic shocks is well understood, progress to include viscous effects into hydraulic theory has been slow. This is of course not surprising if the flow in the liquid layer is turbulent. However, even in the case of laminar flow the phenomena associated with dissipation and surface tension are found to be surprisingly rich. Possible effects include the flow separation, the formation of a roller on top of the fluid layer, the presence of a downstream wavetrain or combinations of these (e.g. [6,19,26,28,29,41]. A complete theoretical picture does not seem to be available at present.

A first important step towards the development of such a picture was taken by Gajjar and Smith [8]. They demonstrated that the jump can be interpreted as the result of a viscous–inviscid interaction where the flow in a thin viscous layer at the wall reacts to the pressure gradient which in turn is induced by the displacement of this viscous layer. The adverse pressure gradient leads to boundary layer separation (which immediately

A. Kluwick (✉) · A. Exner · C. Grinschgl
Institute of Fluid Mechanics and Heat Transfer, Vienna University of Technology, Resselgasse 3/E322, 1040 Wien, Austria
E-mail: alfred.kluwick@tuwien.ac.at

E. A. Cox
School of Mathematical Sciences, University College Dublin, Belfield, Dublin 4, Ireland

excludes the use of classical boundary layer theory) with the inviscid flow domain displaced upwards. This flow scenario is interpreted as a branching of the flow from the upstream unperturbed supercritical state as the flow starts to adjust to downstream conditions. The asymptotic theory developed is similar to that of triple deck theory [16,34,36] where the free stream flow is modified by boundary layer interaction. In [2] the analysis of the hydraulic jump structure is extended to a fully developed viscous upstream profile. Their analysis also includes the effect of surface tension and streamline curvature. In [11] the flow of a thin viscous layer over a finite plate extends the work of [2] who considered only the properties of the interaction region at the leading edge of the jump to include a description of the flow in the whole of a planar hydraulic jump. In all these studies the Froude number characterising the oncoming flow is taken to be sufficiently large so that the flow conditions inside the triple deck region stay supercritical.

The inclusion of viscous fluid effects has a long history (see the pioneering paper of [12] and also [13] for extensive references and discussion). If one considers the modeling of viscous boundary layer effects for free surface flows then there are also extensive results when the unperturbed flow is in a state of rest in contrast to the supercritical case considered here. The bottom shear stress is then included through a convolution integral of the free stream velocity and results in model equations (essentially of KdV type with an integral viscous term) obtained in a variety of contexts including fluid sloshing, solitary waves, undular bores and internal waves in shallow channels (see for example [1,5,14,25]). The effects of dissipation are extended to resonant flows with topography and compared with experiments in [37]. More recently a perturbation approach has been used to incorporate linear boundary layer damping into Boussinesq-type equations [7,22]. In [23] the analysis is extended to include a comparison between numerical solutions for a nonlinear boundary layer model with experimental results. The basis of all these models is a pressure, vertical velocity interaction that ultimately generates a mechanism for energy transfer from an essentially inviscid fluid to a viscous boundary layer on the channel bottom [22,24]. The modelling is also similar to the inclusion of dispersive wall friction effects in acoustic waves (see [15] and references therein).

Here, we use the framework of triple deck theory which includes strong coupling between the boundary layer and the inviscid flow region. In contrast to the classical boundary layer concept it, therefore, is able to account for the effect of upstream influence necessary to resolve the jump discontinuity predicted by hydraulic theory into a smooth profile. Also, boundary layer separation can now be handled and is a feature of the resulting flow generated. However, in contrast to the existing analysis of triple deck flows for large Froude numbers, the present study assumes that the approaching flow is just slightly supercritical with then weak hydraulic jumps. As a consequence, even small disturbances may take the flow into the subcritical regime enabling an asymptotic theory to be formulated to cover the whole flow development from initial upstream state to final downstream states. It is found possible to account for the interaction of weak hydraulic jumps, surface-mounted obstacles and unsteady effects.

2 Problem formulation

We investigate (see Fig. 1) the two-dimensional horizontal channel flow of an incompressible fluid with a free surface at $\tilde{y} = \tilde{h}(\tilde{x}, \tilde{t})$. Incoming upstream flow consists of uniform flow (horizontal velocity $\tilde{U}_0$) with a thin boundary layer (thickness $\tilde{\theta}$) satisfying the no-slip condition on a rigid bottom surface. We are concerned with an analysis of the perturbed flows generated where this incoming flow adjusts now to a new downstream state leading to hydraulic jumps in the fluid. Of primary interest is an investigation of the internal structure of these jumps, which emerges if internal friction is taken into account in the thin bottom boundary layer.

It will be assumed that the upstream flow is marginally supercritical with the Froude number $Fr = \tilde{U}_0/\sqrt{\tilde{g}\tilde{H}}$ (the ratio of the flow speed to the shallow water wave speed) satisfying

$$0 < Fr - 1 \ll 1, \tag{1}$$

where $\tilde{g}$ is the acceleration due to gravity and $\tilde{H}$ is the uniform upstream depth. The change in fluid layer thickness will be small compared to the depth $\tilde{H}$ and this will enable us to construct a weakly nonlinear analysis not only locally, i.e. in the region where the fluid starts to thicken as in [8], but also globally. Our analysis will also be extended to include the additional effect of a varying bottom surface topography ($\tilde{y} = \tilde{s}(\tilde{x}, \tilde{t})$) due to a localized obstacle.

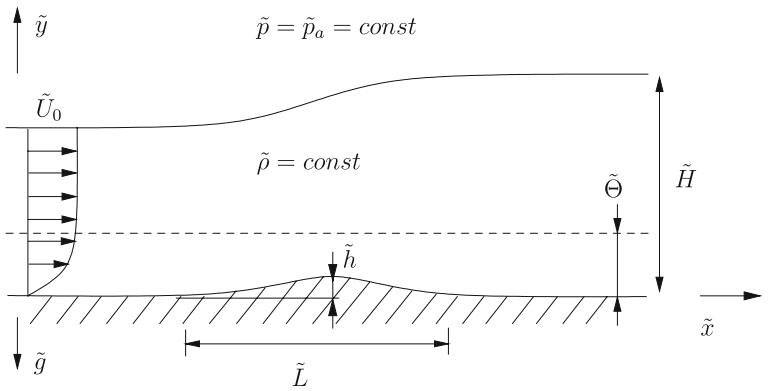

Fig. 1 Problem and notation used for single layer fluid flow over an isolated obstacle

Anticipating that the horizontal length scale $\tilde{L}$ over which the fluid adjustment occurs is large compared to $\tilde{H}$, appropriate non-dimensional quantities are introduced in the usual way:

$$x = \frac{\tilde{x}}{\tilde{L}}, \quad y = \frac{\tilde{y}}{\tilde{H}}, \quad s = \frac{\tilde{s}}{\tilde{H}}, \quad h = \frac{\tilde{h}}{\tilde{H}}, \quad t = \frac{\sqrt{\tilde{g}\tilde{H}}}{\tilde{L}}\tilde{t}, \tag{2}$$

$$u = \frac{\tilde{u}}{\sqrt{\tilde{g}\tilde{H}}}, \quad v = \frac{\tilde{v}}{\sqrt{\tilde{g}\tilde{H}}}\frac{\tilde{L}}{\tilde{H}}, \quad p = \frac{\tilde{p} - \tilde{p}_a}{\tilde{\rho}\tilde{g}\tilde{H}}, \tag{3}$$

where $\tilde{x}$, $\tilde{y}$, $\tilde{u}$, $\tilde{v}$, $\tilde{t}$, $\tilde{p}$, $\tilde{\rho}$ and $\tilde{p}_a$ denote Cartesian coordinates, corresponding velocity components, time, pressure, fluid density and the constant pressure imposed just above the free surface.

The governing equations then assume the form

$$\begin{aligned}
&\frac{\partial u}{\partial x} + \frac{\partial v}{\partial y} = 0,\\
&\frac{\partial u}{\partial t} + u\frac{\partial u}{\partial x} + v\frac{\partial u}{\partial y} = -\frac{\partial p}{\partial x} + \frac{1}{Re}\left(\frac{\tilde{H}^2}{\tilde{L}^2}\frac{\partial^2 u}{\partial x^2} + \frac{\partial^2 u}{\partial y^2}\right),\\
&\frac{\partial v}{\partial t} + u\frac{\partial v}{\partial x} + v\frac{\partial v}{\partial y} = -\frac{\tilde{L}^2}{\tilde{H}^2}\left(\frac{\partial p}{\partial y} + 1\right) + \frac{1}{Re}\left(\frac{\tilde{H}^2}{\tilde{L}^2}\frac{\partial^2 v}{\partial x^2} + \frac{\partial^2 v}{\partial y^2}\right).
\end{aligned} \tag{4}$$

Here, the Reynolds number Re is defined as

$$Re = \frac{\tilde{L}\sqrt{\tilde{g}\tilde{H}}}{\tilde{\nu}}\frac{\tilde{H}^2}{\tilde{L}^2}. \tag{5}$$

where the kinematic viscosity $\tilde{\nu}$ is assumed constant.

In the large Reynolds number limit $Re \gg 1$ considered here, viscous effects are weak globally and of importance primarily in a thin boundary layer adjacent to the wall where the no-slip condition

$$y = s(x,t): \quad u = 0, \quad v = \frac{\partial s}{\partial t} \tag{6}$$

has to be satisfied.

As a consequence, the boundary conditions at the free surface are simply those of inviscid flow:

$$\begin{aligned}
&y = h(x,t): \quad \frac{\partial h}{\partial t} + u\frac{\partial h}{\partial x} - v = 0,\\
&p = -T\frac{\partial^2 h}{\partial x^2}\left(1 + \frac{\tilde{H}^2}{\tilde{L}^2}\left(\frac{\partial h}{\partial x}\right)^2\right)^{-3/2},
\end{aligned} \tag{7}$$

where the non-dimensional parameter $T = \tilde{\sigma}/\tilde{g}\tilde{\rho}\tilde{L}^2$ characterizes the effect of the constant surface tension $\tilde{\sigma}$. Viscous effects in the flow near the free surface can be shown to be $O(Re^{-11/9})$ and will be neglected in comparison to $O(Re^{-4/9})$ terms retained.

3 Derivation of the interaction equations

3.1 Order of magnitude estimates

We consider an induced perturbation of the upstream flow where, as in the case $Fr - 1 = O(1)$ of [8], the flow adjusting to an imposed downstream state results in a triple-deck structure (see Fig. 2). Defining features of this asymptotic structure include viscous perturbations confined to a thin sublayer (lower deck) of the incoming boundary layer with the remaining part of the incoming boundary layer (main deck) modified only passively through an additional inviscid displacement. Adjustment of the incoming inviscid flow region (upper deck) involves an inviscid free-surface flow response to this imposed displacement. The inclusion of this free-surface distortion will modify the viscous–inviscid interactions which otherwise are typical of triple-deck problems (see [16,34,36]).

Estimates for the magnitude of the flow quantities in the lower deck follow from the assumption that the wall shear upstream of the bore is finite, the mass balance and the requirement that inertia, pressure gradient and viscous terms are of equal importance in the streamwise momentum equation. One obtains

$$u \sim \frac{\delta}{\Theta}, \quad v \sim \frac{\delta^2}{\Theta}, \quad \frac{\partial p}{\partial x} \sim \frac{\delta^2}{\Theta^2}, \quad \delta^3 = \frac{\Theta}{Re}, \tag{8}$$

where Θ and δ, respectively, denote the vertical extent of the boundary layer and the lower deck non-dimensionalized with respect to the unperturbed depth $\tilde{H}$ of the liquid.

Guided by other triple-deck problems the flow in the main deck is expected to be inviscid and passive, i.e. not affected by the pressure gradient, in leading order. Furthermore, the deviations from the unperturbed velocity profile $U(y)$ are taken to be of the same order of magnitude as the streamwise velocity component in the lower deck:

$$U(y) - u \sim \frac{\delta}{\Theta}, \quad v \sim \delta. \tag{9}$$

The flow in the upper deck incorporates the distortion of the free-surface $y = h(x,t)$ under the near-critical flow conditions given by $0 < Fr - 1 \ll 1$. For critical flows, disturbances induced in the upper deck by the imposed boundary layer displacement cannot propagate away from the interaction region. This resonance results then in the generation of strong nonlinear responses. We anticipate that a boundary layer displacement of $O(\delta)$ will achieve a balance with leading order quadratic nonlinear terms. Hence we expect

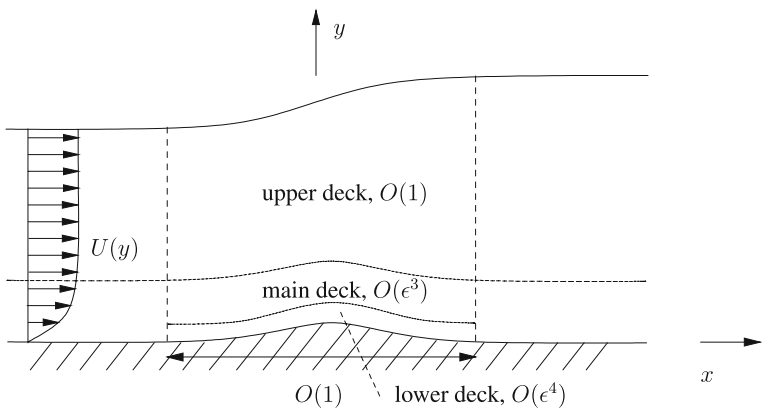

Fig. 2 Triple deck structure of interaction region

the nonlinear response to scale with $\delta^{1/2}$. Evaluation of the mass balance, the streamwise momentum equation and the boundary conditions at the free surface then yields

$$1 - h \sim U(y) - u \sim v \sim \frac{\partial p}{\partial x} \sim T \sim \delta^{1/2}, \tag{10}$$

where we have also scaled the parameter T to incorporate surface tension effects.

We also consider the *small amplitude, shallow-water* limit where nonlinear amplitude disturbances, $O(\delta^{1/2})$, and streamline curvature effects identified with the nondimensional depth $\tilde{H}^2/\tilde{L}^2$ in Eqs. (4) are scaled by

$$\frac{\tilde{H}^2}{\tilde{L}^2} = \delta^{1/2}. \tag{11}$$

Vertical scales for surface bottom topography consistent with the proposed flow structure give a maximum obstacle height

$$s_{\max} \sim O(\delta)\,. \tag{12}$$

The assumption that the main deck is passive (suggested by previous triple deck studies and confirmed in Sect. 3.2 to yield a fully self-consistent flow description) gives equivalent estimates in (8) and (10) for the pressure gradient $\partial p/\partial x$ which determines the boundary layer thickness relations

$$\delta = \Theta^{4/3}. \tag{13}$$

In terms of the expansion parameter

$$\varepsilon = Re^{-1/9} \tag{14}$$

Eq. (8) then provides the boundary layer thickness estimates

$$\Theta = O(\varepsilon^3), \quad \delta = O(\varepsilon^4) \tag{15}$$

and leads to estimates of the flow quantities in (8)–(10) which form the basis of the asymptotic expansions.

3.2 Asymptotic analysis

3.2.1 Upper Deck Expansions

Based on the results obtained in Sect. 3.1 the field quantities in the upper deck are expanded in the form

$$\begin{aligned}
u &= 1 + \varepsilon^2(u_{02} + u_2(x,\tau)) + \varepsilon^3 u_3(x,\tau) + \varepsilon^4 u_4(x,y,\tau) + \cdots,\\
v &= \varepsilon^2 v_2(x,y,\tau) + \varepsilon^3 v_3(x,y,\tau) + \varepsilon^4 v_4(x,y,\tau) + \cdots,\\
p &= p_0(y) + \varepsilon^2 p_2(x,\tau) + \varepsilon^3 p_3(x,\tau) + \varepsilon^4 p_4(x,y,\tau) + \cdots,\\
h &= 1 + \varepsilon^2 h_2(x,\tau) + \varepsilon^3 h_3(x,\tau) + \varepsilon^4 h_4(x,\tau) + \cdots,
\end{aligned} \tag{16}$$

where ε is given by (14) and $p_0(y) = 1 - y$ is simply the hydrostatic pressure.

The detuning parameter u_{02} accounts for the (small) deviation of the Froude number from the critical value 1:

$$u_{02} = \frac{Fr - 1}{\varepsilon^2}. \tag{17}$$

Furthermore, we look for solutions that evolve on the slow time scale $\tau = \varepsilon^2 t$.

That the condition $Fr - 1 = O(\varepsilon^2)$ expressed by Eq. (17) can be met is indeed a nontrivial matter and requires a careful investigation of the displacement effect exerted by the boundary layer upstream of the interaction region on the outer inviscid flow. In brief, an upstream boundary layer of thickness $O(\varepsilon^3)$ will eventually lead to a perturbed velocity of $O(\varepsilon^{3/2})$. This is larger than the $O(\varepsilon^2)$ assumed and a singularity will occur in

the flow upstream of the interaction region described in this paper. A slight lowering of the bottom topography or suction in the development region can ensure that the velocity perturbation is of the right order.

Flows are perturbed by boundary layer displacements generated in the lower deck and transmitted by the main deck. This is accounted for by requiring that

$$\lim_{y\to 0} v(x, y, \tau) = \varepsilon^4 v_{bl}(x, \tau), \tag{18}$$

with v_{bl} determined by matching with the main deck solutions.

Asymptotic solutions to (4) are obtained on substituting in expansions (16) assuming the scalings developed in Sect. 3.1 and imposing the free surface boundary conditions (7).

One obtains at $O(\varepsilon^2)$ and $O(\varepsilon^3)$

$$v_2 = -y\frac{\partial u_2}{\partial x}, \quad p_2 = h_2 = -u_2, \tag{19}$$

$$v_3 = -y\frac{\partial u_3}{\partial x}, \quad p_3 = h_3 = -u_3, \tag{20}$$

where the velocity disturbances u_2, u_3 remain arbitrary at this stage of the analysis. In order to determine $u_2(x, \tau)$ it is necessary to consider the terms of $O(\varepsilon^4)$ in (16). To this end it is convenient to write

$$\begin{aligned} u_4 &= U_4(x, y, \tau) + \overline{u}_4(x, \tau), \\ v_4 &= V_4(x, y, \tau) + \overline{v}_4(x, y, \tau), \\ p_4 &= P_4(x, y, \tau) + \overline{p}_4(x, y, \tau), \end{aligned} \tag{21}$$

where U_4, V_4 and P_4 are required to satisfy

$$\begin{aligned} &\frac{\partial U_4}{\partial x} + \frac{\partial V_4}{\partial y} = 0, \\ &\frac{\partial U_4}{\partial x} + \frac{\partial P_4}{\partial x} = 0, \\ &\frac{\partial v_2}{\partial x} + \frac{\partial P_4}{\partial y} = 0, \end{aligned} \tag{22}$$

so that

$$\begin{aligned} &\frac{\partial \overline{u}_4}{\partial x} + \frac{\partial \overline{v}_4}{\partial y} = 0, \\ &\frac{\partial \overline{u}_4}{\partial x} + \frac{\partial \overline{p}_4}{\partial x} = -\frac{\partial u_2}{\partial \tau} - u_2\frac{\partial u_2}{\partial x} - u_{02}\frac{\partial u_2}{\partial x}, \\ &\frac{\partial \overline{p}_4}{\partial y} = 0. \end{aligned} \tag{23}$$

The solution of Eq. (22) is given by

$$U_4 = -P_4 = \frac{y^2}{2}\frac{\partial^2 h_2}{\partial x^2}, \quad V_4 = -\frac{y^3}{6}\frac{\partial^3 h_2}{\partial x^3}. \tag{24}$$

Using the first of Eqs. (23) the fourth order contributions to v and p can be written as

$$v_4 = -\frac{y^3}{6}\frac{\partial^3 h_2}{\partial x^3} - y\frac{\partial \overline{u}_4}{\partial x} + v_{b\ell}(x, \tau), \quad p_4 = -\frac{y^2}{2}\frac{\partial^2 h_2}{\partial x^2} + \overline{p}_4, \tag{25}$$

where $v_{b\ell}(x, \tau)$ yet unknown accounts for the displacement effect of the inner layers. Evaluation of the boundary conditions (7) at $O(\varepsilon^4)$ yields

$$\frac{\partial h_4}{\partial x} + \frac{\partial \overline{u}_4}{\partial x} = -\frac{\partial h_2}{\partial \tau} - u_{02}\frac{\partial h_2}{\partial x} - u_2\frac{\partial h_2}{\partial x} - h_2\frac{\partial u_2}{\partial x} - \frac{1}{6}\frac{\partial^3 h_2}{\partial x^3} + v_{b\ell} \tag{26}$$

and

$$\overline{p}_4 = h_4 - \hat{T}\frac{\partial^2 h_2}{\partial x^2} + \frac{1}{2}\frac{\partial^2 h_2}{\partial x^2}, \tag{27}$$

where

$$\hat{T} = \frac{T}{\varepsilon^2} \tag{28}$$

denotes the properly scaled Weber number.

Using Eq. (27) to eliminate $\overline{p}_4$ from the second of Eqs. (23) generates a second relationship for the expression on the left hand side of Eq. (26):

$$\frac{\partial h_4}{\partial x} + \frac{\partial \overline{u}_4}{\partial x} = -\frac{\partial u_2}{\partial \tau} - u_{02}\frac{\partial u_2}{\partial x} - u_2\frac{\partial u_2}{\partial x} + \hat{T}\frac{\partial^3 h_2}{\partial x^3} - \frac{1}{2}\frac{\partial^3 h_2}{\partial x^3} \tag{29}$$

and, therefore, shows that the second order quantities u_2, h_2 have to satisfy a solvability condition which can be cast into the form

$$\frac{\partial p_2}{\partial \tau} + u_{02}\frac{\partial p_2}{\partial x} - \frac{3}{2}p_2\frac{\partial p_2}{\partial x} + \frac{3\hat{T}-1}{6}\frac{\partial^3 p_2}{\partial x^3} = \frac{1}{2}v_{b\ell} \tag{30}$$

by taking into account the results summarized in Eqs. (19), (20).

With $p_2 = h_2$ Eq. (30) also describes the evolution of the free surface profile. The term v_{bl} represents the boundary layer displacement effect which is not know a priori but involves solutions of the lower deck equation which in turn are dependent on $p_2(x, \tau)$. When, in contrast, v_{bl} is a prescribed function, then (30) arises in transcritical flows over bottom topography [10].

3.2.2 Main Deck Expansions

Appropriate expansions of the field quantities in the main deck region are

$$\begin{aligned} u &= U_0(\overline{y}) + \varepsilon\overline{u}_1(x, \overline{y}, \tau) + \cdots, \\ v &= \varepsilon^4\overline{v}_4(x, \overline{y}, \tau) + \cdots, \\ p &= 1 + \varepsilon^2\overline{p}_2(x, \tau) + \cdots, \end{aligned} \tag{31}$$

where

$$\overline{y} = \frac{y}{\varepsilon^3} = O(1). \tag{32}$$

As in other triple deck problems, the leading order solution describes the passive shift of the unperturbed velocity profile $U_0(\overline{y})$ in the lateral direction characterized by the displacement function $A_1(x, \tau)$:

$$\overline{u}_1 = A_1(x, \tau)U_0'(\overline{y}), \quad \overline{v}_4 = -U_0(\overline{y})\frac{\partial A_1}{\partial x}(x, \tau). \tag{33}$$

Matching with the results holding in the upper deck yields

$$v_{b\ell} = -\frac{\partial A_1}{\partial x} \tag{34}$$

and

$$\overline{p}_2 = p_2. \tag{35}$$

3.2.3 Lower Deck Expansions

Finally, in the lower deck region u, v and p are expanded as

$$\begin{aligned} u &= \varepsilon u_1^*(x, y^*, \tau) + \cdots, \\ v &= \varepsilon^5 v_5^*(x, y^*, \tau) + \cdots, \\ p &= 1 + \varepsilon^2 p_2^*(x, \tau) + \cdots, \end{aligned} \tag{36}$$

with

$$y^* = \frac{y}{\varepsilon^4} = O(1). \tag{37}$$

From Eqs. (12) and (15) the surface-mounted obstacle is described by $y = \varepsilon^4 s_4(x)$. Owing to the slow variations of the field quantities in the upper deck the flow close to the solid wall is quasi-steady:

$$\begin{aligned} &\frac{\partial u_1^*}{\partial x} + \frac{\partial v_5^*}{\partial y^*} = 0\,, \\ &u_1^* \frac{\partial u_1^*}{\partial x} + v_5^* \frac{\partial u_1^*}{\partial y^*} = -\frac{\partial p_2^*}{\partial x^*} + \frac{\partial^2 u_1^*}{\partial y^{*2}}. \end{aligned} \tag{38}$$

The boundary conditions include the no-slip condition at the surface-mounted obstacle

$$y^* = s_4(x, \hat{t}\,): \quad u_1^* = v_5^* = 0 \tag{39}$$

as well as the requirement that the disturbances caused by the obstacle and/or bore decay upstream

$$x \to -\infty: \quad u_1^* = \lambda y^*. \tag{40}$$

Here, the constant λ characterizes the wall shear in the unperturbed boundary layer. Matching of (36) taking into account (37) with the main deck solution requires

$$u_1^* = \lambda \left(y^* + A_1(x, \tau)\right) \quad \text{as} \quad y^* \to \infty \tag{41}$$

and

$$p_2^*(x, \tau) = \overline{p}_2(x, \tau). \tag{42}$$

Consequently, the pressure acting in the lower deck is determined by Eq. (30) where $v_{b\ell}$ is replaced with $-\partial A_1/\partial x$, which closes the problem.

As usual it is convenient to reduce the number of parameters entering the lower deck problem by introducing transformed quantities. A suitable choice is

$$\begin{aligned} &x = \lambda^{-2} a^{3/2} X, \quad y^* = \lambda^{-1} a^{1/2} (Y + F), \quad \tau = \lambda^{-2} a^{3/2} |u_{02}|^{-1} \hat{t}, \\ &u_1^* = a^{1/2} U, \quad v_5^* = \lambda a^{-1/2} \left(V - U \frac{\partial F}{\partial X}\right), \quad p_2^* = a P, \\ &A_1 = \lambda^{-1} a^{1/2} A, \quad s_4^* = \lambda^{-1} a^{1/2} F, \quad a = \frac{2}{3} |u_{02}|. \end{aligned} \tag{43}$$

In summary then, the combined triple-deck problem incorporating free surface distortion is given by the coupled system of equations and boundary conditions

$$\frac{\partial U}{\partial X} + \frac{\partial V}{\partial Y} = 0\,, \tag{44}$$

$$U \frac{\partial U}{\partial X} + V \frac{\partial U}{\partial Y} = -\frac{\partial P}{\partial X} + \frac{\partial^2 U}{\partial Y^2}, \tag{45}$$

$$Y = 0: \quad U = V = 0, \tag{46}$$

$$X \to -\infty: \quad U = Y, \tag{47}$$

$$Y \to \infty: \quad U = Y + A, \tag{48}$$

$$\frac{\partial P}{\partial \hat{t}} + \frac{\partial P}{\partial X} - P\frac{\partial P}{\partial X} - \frac{W}{2}\frac{\partial^3 P}{\partial X^3} = -\frac{\Lambda}{2}\frac{\partial (A-F)}{\partial X}, \tag{49}$$

where

$$W = (1-3\hat{T})\frac{9}{8}\frac{\lambda^4}{u_{02}^4}, \quad \Lambda = \sqrt{\frac{3}{2}}\frac{1}{\lambda u_{02}^{3/2}}. \tag{50}$$

The parameter W characterizes the relative importance of detuning and surface tension and Λ provides for streamline curvature and boundary layer displacement effects in the interaction equation (49).

In the limiting case of large Froude number with small non-resonant pressure disturbances equation (49) with F and $W = 0$ reduces in the stationary state to

$$P = -\frac{\Lambda}{2}A(x) \tag{51}$$

which corresponds to the $Fr \to 1$ limit of the interaction law in [8]. Their analysis involves the non-resonant triple-deck problem (44)–(49) with interaction law (51).

4 Results

4.1 Linear flow response

Although the main thrust of the present investigation is directed towards the internal structure of hydraulic jumps it is nevertheless useful to study first the behavior of disturbances that are too weak to generate this fully nonlinear phenomenon as it is expected to provide insight into the initial departure from the unperturbed state as $X \to -\infty$ and to shed light on the question whether unsteady perturbations caused, for example, by a suddenly formed surface-mounted obstacle settle down to a steady response in the limit $\hat{t} \to \infty$. To this end we introduce the small perturbation parameter $\alpha \ll 1$ and expansions

$$\begin{aligned} &U = Y + \alpha U_1 + \cdots, \quad V = \alpha V_1 + \cdots, \quad P = \alpha P_1 + \cdots, \\ &A = \alpha A_1 + \cdots, \quad F = \alpha F_1 + \ldots \end{aligned} \tag{52}$$

In leading order one then obtains the linearized boundary layer equations

$$\frac{\partial U_1}{\partial X} + \frac{\partial V_1}{\partial Y} = 0, \tag{53}$$

$$Y\frac{\partial U_1}{\partial X} + V_1 = -\frac{\mathrm{d}P_1}{\mathrm{d}X} + \frac{\partial^2 U_1}{\partial Y^2}, \tag{54}$$

subject to the boundary and matching conditions

$$U_1 = V_1 = 0 \quad \text{on} \quad Y = 0, \tag{55}$$

$$U_1 = A_1 \quad \text{for} \quad Y \to \infty, \tag{56}$$

$$U_1 = 0 \quad \text{for} \quad X \to \infty, \tag{57}$$

and the interaction law

$$\frac{\partial P_1}{\partial \hat{t}} + \frac{\partial P_1}{\partial X} - \frac{W}{2}\frac{\partial^3 P_1}{\partial X^3} = -\frac{\Lambda}{2}\frac{\partial}{\partial X}(A_1 - F_1). \tag{58}$$

Following [36] the linearized momentum equation (54) is differentiated with respect to Y yielding a single equation for the perturbation of the shear stress $\tau_1 = \partial U_1/\partial Y$:

$$Y\frac{\partial \tau_1}{\partial X} = \frac{\partial^2 \tau_1}{\partial Y^2}, \tag{59}$$

which can be solved using Fourier transformation. Introducing the Fourier transform

$$\overline{f}(\omega, Y, \hat{t}) = \frac{1}{\sqrt{2\pi}}\int_{-\infty}^{\infty} f(X, Y\hat{t})e^{-i\omega X}\mathrm{d}X \tag{60}$$

of the field quantity $f(X, Y, \hat{t})$, one finds

$$\overline{\tau}_1 = B(\omega, \hat{t}) \, \mathrm{Ai}\left((i\omega)^{1/3} Y\right). \tag{61}$$

Here $\mathrm{Ai}(s)$ denotes the Airy function. The yet arbitrary function $B(\omega, \hat{t})$ is determined by the matching and boundary conditions (55)–(57) and the interaction law (58). It can, in general, not be expressed in closed form. However, if we consider wall-mounted obstacles which are generated suddenly at $\hat{t} = 0$, i.e.

$$\begin{aligned} F_1(X, \hat{t}) &= C(\hat{t}) S_1(X), \\ C(\hat{t}) &= \begin{cases} 0, & \hat{t} < 0 \\ 1, & \hat{t} \geq 0 \end{cases} \end{aligned} \tag{62}$$

one obtains the analytic expression

$$B(\omega, \hat{t}) = \frac{3(i\omega)^{5/3}}{\phi a(\omega)} \left(1 - e^{-a(\omega)\hat{t}}\right) \overline{S}_1(\omega), \tag{63}$$

$$a(\omega) = -\frac{1}{2}\frac{\omega^{4/3}}{\phi} + i\left(\frac{\vartheta}{\phi}\omega - \frac{\sqrt{3}}{2}\frac{\omega^{4/3}}{\phi}\right) \tag{64}$$

with the constants

$$\phi = \frac{6\mathrm{Ai}'(0)}{\Lambda}, \tag{65}$$

$$\vartheta = \phi\left(1 + \frac{W}{2}\omega^2\right). \tag{66}$$

Back transformation into the X, Y-space then leads to

$$\begin{aligned} \tau_{w1}(X, \hat{t}) = \tau_1(X, 0, \hat{t}) = {} & \frac{3\sqrt{2}Ai(0)}{\sqrt{\pi}} \int_0^\infty \bar{S}_1(\omega) \frac{\omega \cos\left(\omega X + \frac{\pi}{6}\right) + \vartheta\omega^{\frac{2}{3}} \cos\left(\omega X + \frac{\pi}{3}\right)}{\omega^{\frac{2}{3}} + \sqrt{3}\vartheta\omega^{\frac{1}{3}} + \vartheta^2} \, \mathrm{d}\omega \\ & - \frac{3\sqrt{2}Ai(0)}{\sqrt{\pi}} \int_0^\infty \bar{S}_1(\omega) \exp\left(\frac{\omega^{\frac{4}{3}}}{2\phi}\hat{t}\right) \frac{\omega \cos(\omega X + \frac{\pi}{6} - \zeta) + \vartheta\omega^{\frac{2}{3}} \cos(\omega X + \frac{\pi}{3} - \zeta)}{\omega^{\frac{2}{3}} + \sqrt{3}\vartheta\omega^{\frac{1}{3}} + \vartheta^2} \, \mathrm{d}\omega, \end{aligned} \tag{67}$$

$$\zeta = \zeta(\omega, \hat{t}) = \frac{\omega}{\phi}\left(\vartheta + \frac{\sqrt{3}}{2}\omega^{1/3}\right)\hat{t} \tag{68}$$

as well as the results

$$\begin{aligned} P_1(X, \hat{t}) = {} & \frac{3\sqrt{2}Ai'(0)}{\sqrt{\pi}} \int_0^\infty \bar{S}_1(\omega) \frac{\omega^{\frac{1}{3}} \cos\left(\omega X - \frac{\pi}{6}\right) + \vartheta \cos(\omega X)}{\omega^{\frac{2}{3}} + \sqrt{3}\vartheta\omega^{\frac{1}{3}} + \vartheta^2} \, \mathrm{d}\omega \\ & - \frac{3\sqrt{2}Ai'(0)}{\sqrt{\pi}} \int_0^\infty \bar{S}_1(\omega) \exp\left(\frac{\omega^{\frac{4}{3}}}{2\phi}\hat{t}\right) \\ & \times \frac{\omega^{\frac{1}{3}} \cos(\omega X - \frac{\pi}{6} - \frac{\hat{t}}{\phi}(\omega\vartheta + \frac{\sqrt{3}}{2}\omega^{\frac{4}{3}})) + \vartheta \cos(\omega X - \frac{\hat{t}}{\phi}(\omega\vartheta + \frac{\sqrt{3}}{2}\omega^{\frac{4}{3}}))}{\omega^{\frac{2}{3}} + \sqrt{3}\vartheta\omega^{\frac{1}{3}} + \vartheta^2} \, \mathrm{d}\omega, \end{aligned} \tag{69}$$

$$\begin{aligned} A_1(X, \hat{t}) = {} & \frac{\sqrt{2}}{\sqrt{\pi}} \int_0^\infty \bar{S}_1(\omega) \frac{\omega^{\frac{2}{3}} \cos(\omega X) + \vartheta\omega^{\frac{1}{3}} \cos(\omega X + \frac{\pi}{6})}{\omega^{\frac{2}{3}} + \sqrt{3}\vartheta\omega^{\frac{1}{3}} + \vartheta^2} \, \mathrm{d}\omega \\ & - \frac{\sqrt{2}}{\sqrt{\pi}} \int_0^\infty \bar{S}_1(\omega) \exp\left(\frac{\omega^{\frac{4}{3}}}{2\phi}\hat{t}\right) \frac{\omega^{\frac{2}{3}} \cos(\omega X - \zeta) + \vartheta\omega^{\frac{1}{3}} \cos(\omega X + \frac{\pi}{6} - \zeta)}{\omega^{\frac{2}{3}} + \sqrt{3}\vartheta\omega^{\frac{1}{3}} + \vartheta^2} \, \mathrm{d}\omega \end{aligned} \tag{70}$$

for the leading order perturbations of $P(X,\hat{t})$ and $A(X,\hat{t})$. Taking into account that $\Lambda \geq 0$ and $\mathrm{Ai}'(0) = -(3^{1/3}\,\Gamma(1/3))^{-1} < 0$ it follows immediately that the time-dependent terms in Eqs. (67), (69) and (70) decay with increasing time $\hat{t}$ for all values X so that a steady flow response

$$\begin{aligned}
\tau_{w_1}(X) &= \frac{3Ai(0)}{\sqrt{\pi}} \int_0^\infty \exp\left(\frac{-\omega^2}{4}\right) \frac{\omega\cos(\omega X + \frac{\pi}{6}) + \vartheta\omega^{\frac{2}{3}}\cos(\omega X + \frac{\pi}{3})}{\omega^{\frac{2}{3}} + \sqrt{3}\vartheta\omega^{\frac{1}{3}} + \vartheta^2}\,\mathrm{d}\omega, \\
P_1(X) &= \frac{3Ai'(0)}{\sqrt{\pi}} \int_0^\infty \exp\left(\frac{-\omega^2}{4}\right) \frac{\omega^{\frac{1}{3}}\cos(\omega X - \frac{\pi}{6}) + \vartheta\cos(\omega X)}{\omega^{\frac{2}{3}} + \sqrt{3}\vartheta\omega^{\frac{1}{3}} + \vartheta^2}\,\mathrm{d}\omega, \\
A_1(X) &= \frac{1}{\sqrt{\pi}} \int_0^\infty \exp\left(\frac{-\omega^2}{4}\right) \frac{\omega^{\frac{2}{3}}\cos(\omega X) + \vartheta\omega^{\frac{1}{3}}\cos(\omega X + \frac{\pi}{6})}{\omega^{\frac{2}{3}} + \sqrt{3}\vartheta\omega^{\frac{1}{3}} + \vartheta^2}\,\mathrm{d}\omega
\end{aligned} \tag{71}$$

is approached asymptotically as $\hat{t}$ tends to infinity.

As a specific example we consider a Gaussian hump centred at $X = X_0$:

$$S_1(X) = e^{-a(X-X_0)^2}, \tag{72}$$

where $a > 0$. Figure 3 displays the temporal evolution of the pressure disturbances $P_1(X,\hat{t})$ for $W = \Lambda = 1$. It is seen that the sudden emergence of the hump at $\hat{t} = 0$ causes the formation of a wavetrain on its lee side which—as the flow stays supercritical throughout—propagates downstream and decays due to viscous dissipation. As a consequence, a steady state is approached in the limit $\hat{t} \to \infty$. The distributions of P_1, A_1, τ_{w1} characterizing this final steady state are depicted in Fig. 4. Similar to the predictions of purely hydraulic theory the positive displacement of the fluid exerted by the obstacle causes the pressure to rise initially before it drops and returns to the unperturbed level. Also, as to be expected from classical boundary layer theory, the initial pressure increase leads to a reduction of the wall shear while the acceleration of the fluid resulting from the subsequent pressure drop results in a local maximum of τ_{w1}. In contrast to purely hydraulic theory, however, the obstacle exhibits an upstream influence which can be determined from Eqs. (67), (69), (70) by taking the limit $X \to -\infty$ using the residue theorem or more directly by following Lighthill's [20] and Stewartson's [36] analysis of upstream influence in supersonic boundary layers, considering disturbances of the incoming uniform flow of the form

$$U \sim Y - a_1 e^{\kappa X} f'(Y) + \cdots, \quad V \sim a_1\kappa e^{\kappa X} f(Y) + \cdots, \quad P \sim a_1 e^{\kappa X} + \cdots. \tag{73}$$

The solution of the boundary layer equations (44), (45) satisfying the no-slip conditions (46) is then given by

$$f'(Y) = -\frac{\kappa^{2/3}}{\mathrm{Ai}'(0)} \int_0^Y \mathrm{Ai}(z\kappa^{1/3})\mathrm{d}z. \tag{74}$$

Evaluation of the matching condition (48) leads to the well-known result for the displacement function

$$A \sim -Ca_1\kappa^{1/3}e^{\kappa X}, \quad C = -\frac{1}{3\mathrm{Ai}'(0)}. \tag{75}$$

Finally, substitution of the expressions for P and A into the linearized form of the interaction law (49) yields the dispersion relation

$$1 - \frac{C\Lambda}{2}\kappa^{1/3} - \frac{W}{2}\kappa^2 = 0, \tag{76}$$

which determines $\kappa(W,\Lambda)$ in (73). Real solutions exist for

$$W \geq W_c = -\frac{C^6\Lambda^6}{32}\frac{5^5}{6^6}. \tag{77}$$

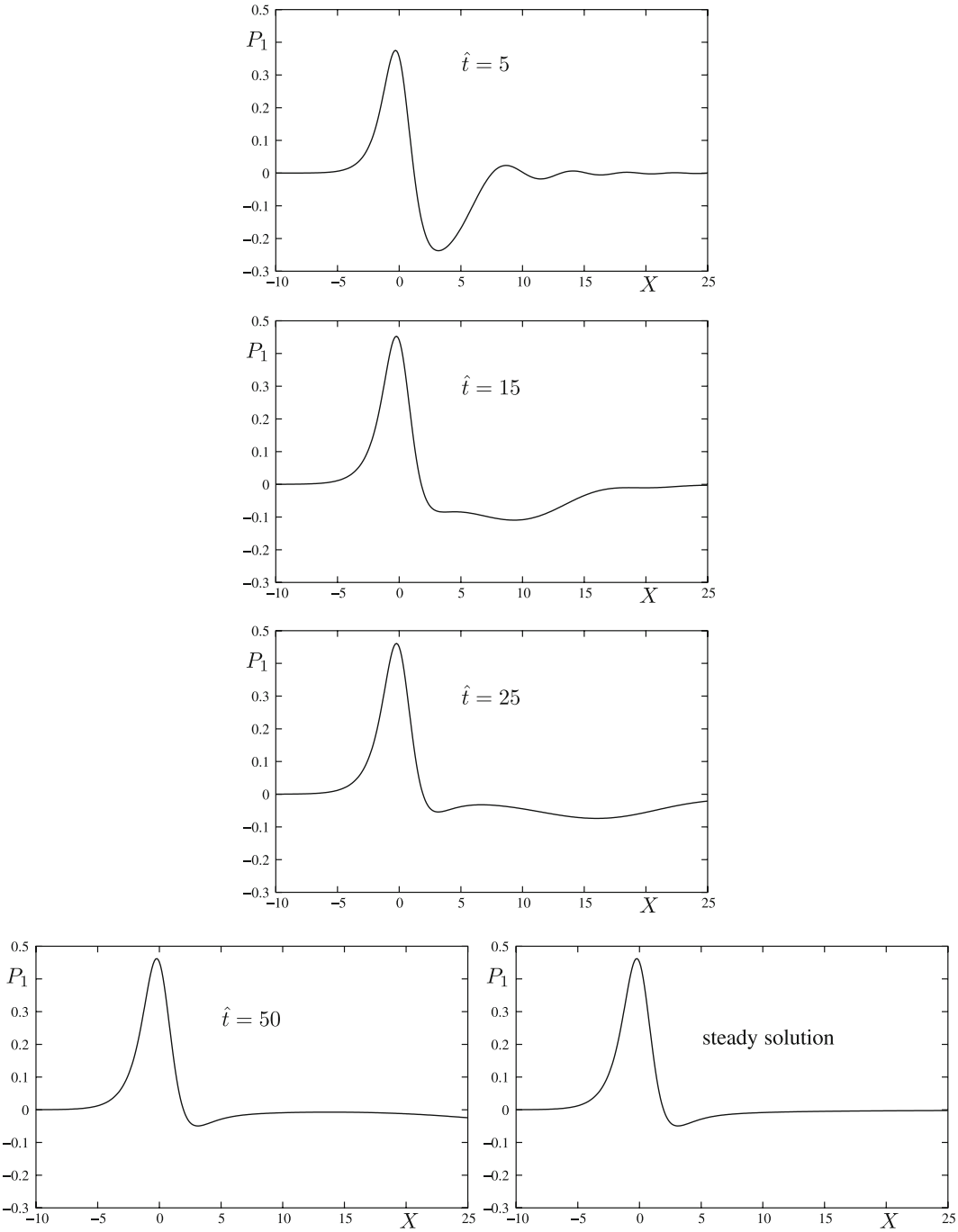

Fig. 3 Temporal evolution of the leading order pressure disturbances P_1 generated by a Gaussian hump centred at $X = 0$ for $W = \Lambda = 1$

The parameter κ describes the initial exponential growth of the disturbance and for positive W is uniquely given by (76). A graph of the dispersion relationship is depicted in Fig. 5. Here use has been made of the fact that the solutions of Eq. (76) reduce to a single curve when expressed in terms of the transformed variables $\overline{\kappa} = C^3\Lambda^3\kappa/8$, $W = 32W/(C^6\Lambda^6)$.

The physically important result that unsteady disturbances generated all of a sudden settle down to a steady state has been inferred so far from the structure of the closed form solution (67)–(70). However, this formal deduction does not apply if one considers more complex body shapes and associated time histories. Also, it

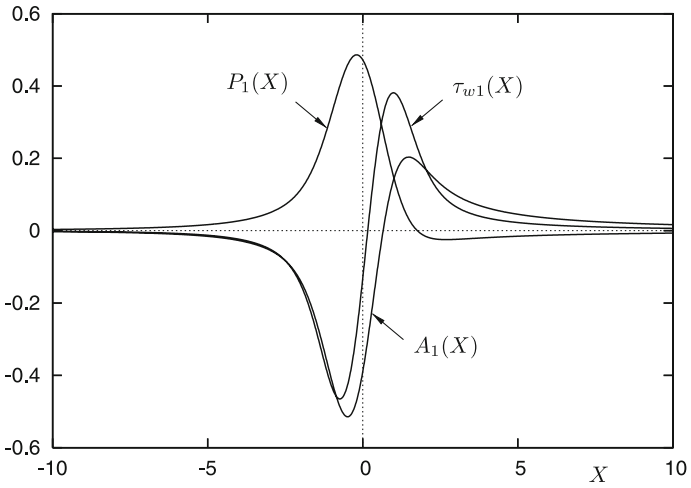

Fig. 4 Steady flow: leading order perturbations of the wall pressure P_1, the wall shear τ_{w1} and the displacement function A_1

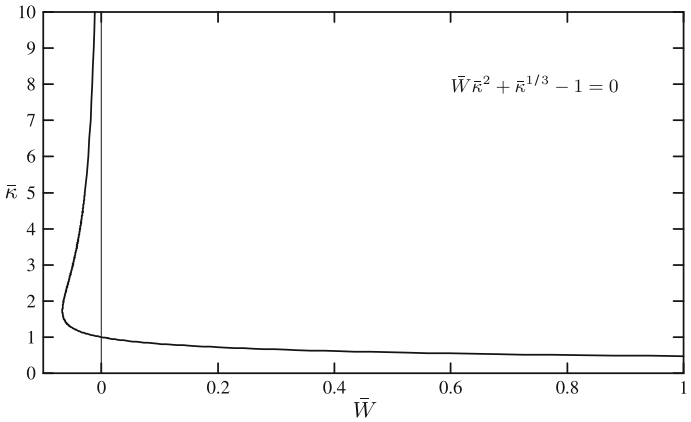

Fig. 5 Graph of dispersion relation (76)

does not shed light on the mechanism by which the unsteady part of the flow motion is damped out in the limit $\hat{t} \to \infty$. Obviously, this mechanism will be related to the occurrence of the perturbation displacement thickness in the interaction relationship (49), but how? Here the key observation is that the Fourier transform $\overline{S}_1(\omega)$ can easily be eliminated from the results for $\overline{A}_1(\omega, \hat{t})$ and $\overline{P}_1(\omega, \hat{t})$ to yield the relationship

$$\overline{A}(\omega, \hat{t}) = \frac{(i\omega)^{1/3}}{3\mathrm{Ai}'(0)} \overline{P}_1(\omega, \hat{t}), \tag{78}$$

whose steady counterpart has been derived much earlier in the different context of transonic shock boundary layer interactions [4]. Application of the convolution theorem then yields

$$A_1(X, \hat{t}) = \frac{1}{3\mathrm{Ai}'(0)\Gamma(\frac{2}{3})} \int_{-\infty}^{X} \frac{1}{(X - X')^{1/3}} \frac{\partial P_1(X', \hat{t})}{\partial X'} \, \mathrm{d}X'. \tag{79}$$

Using the definition of the fractional derivative of order p (e.g. [27])

$$\frac{\partial^p f}{\partial X^p} = \frac{1}{\Gamma(1-p)} \int_{-\infty}^{X} \frac{1}{(X - X')^p} \frac{\partial f}{\partial X'} \mathrm{d}X', \tag{80}$$

where $\Gamma(p)$ is the Gamma function and f is a physical quantity dependent on a space variable X and time $\hat{t}$, Eq. (79) can also be written in the form

$$A_1 = \frac{1}{3\mathrm{Ai}'(0)} \frac{\partial^{1/3} P_1}{\partial X^{1/3}}. \tag{81}$$

Finally, by substituting Eq. (81) into the linearized form (58) of the interaction equation one obtains the single transport equation

$$\frac{\partial P_1}{\partial \hat{t}} + \frac{\partial P_1}{\partial X} - \frac{W}{2} \frac{\partial^3 P_1}{\partial X^3} = -\frac{\Lambda}{6\mathrm{Ai}'(0)} \frac{\partial^{4/3} P}{\partial X^{4/3}} + \frac{\Lambda}{2} \frac{\partial F_1}{\partial X}, \tag{82}$$

which governs the spatial and temporal evolution of the induced pressure disturbances $P_1(X, \hat{t})$. According to [40] the first term on the right-hand side acts as a diffusive term if—as in the present case—the order p of the fractional derivative satisfies the condition $0 < p - 1 < 1$ which provides a rigorous explanation why flow perturbations caused by a surface-mounted obstacle whose shape does not change in the limit $\hat{t} \to \infty$ approach a steady state as observed first for the specific case (62). Interestingly, Eq. (81) can be shown to hold also in cases where weakly nonlinear effects come into play provided that the characteristic wavelength is sufficiently large. This is especially important for two layer flows where it may lead to the formation of non-classical hydraulic jumps as will be shown in a separate study presenting numerical solutions of appropriately generalized forms of Eq. (82).

4.2 Nonlinear eigensolutions—bores

The lower deck problem (44)–(49) has to be solved numerically in general even in the case of steady flow to which the following considerations will be restricted. In this connection, it is useful to investigate the interaction law (49) in more detail. Specifically, we assume that the dispersive term is negligibly small as $W \to 0$ and that P and A are independent of $\hat{t}$. As a consequence, Eq. (49) with $F = 0$ can immediately be integrated to yield the algebraic relation

$$P(X) = 1 \pm \sqrt{1 + \Lambda A(X)}. \tag{83}$$

An interaction law of this form arises in transonic flows in slender channels (see [17]). When A is a given prescribed function then (83) also occurs in shallow-water near-critical flows over bottom topography in the hydraulic limit with P from (19) identified with the free surface displacement. In this case the bottom topography is described by $-\Lambda A$. In Fig. 6 the plot of P $(=3h_2/(2u_{02}))$ versus ΛA identifies critical conditions at $P = 1$, $A = -1/\Lambda$ and, as ΛA increases, a supercritical branch where P increases and a subcritical branch where P decreases. Also it should be noted that a pressure jump between the subcritical and supercritical branches agrees with pressure jumps across weak bores when hydraulic theory is applied to (49). Indicated in Fig. 6 is a jump from an undisturbed upstream supercritical state ($P = 0$) to a downstream subcritical state ($P = 2$). This raises the possibility that the lower deck problem admits eigensolutions, i.e. nontrivial solutions which, in turn, through the coupling (48) generates displacements $-\Lambda A$ enabling the downstream and upstream states of such jumps to be connected along the portion of the curve (83) which passes through the critical point, thereby generating an internal viscous structure. The above considerations will be confirmed by numerical calculations.

For the stationary problem, the full coupling equation (49) with $F \equiv 0$ can also be integrated to yield

$$-P + \frac{1}{2}P^2 + \frac{W}{2} \frac{\mathrm{d}^2 P}{\mathrm{d}X^2} = \frac{\Lambda}{2} A, \tag{84}$$

where P vanishes in the unperturbed state.

The system of equations (44)–(48) and (84) has been solved with a finite difference method using a Crank–Nicholson scheme and a marching procedure in the main stream (i.e. positive X) direction. The pressure gradient $\mathrm{d}P/\mathrm{d}X$ has been introduced as a new dependent variable so that only first derivatives with respect to X appear in (84) as required by the Crank–Nicholson scheme. The matching condition (48) has been replaced by

$$\frac{\partial U}{\partial Y}(X, Y_{\max}) = 1 \tag{85}$$

and a value $Y_{\max}$ has been determined such that (85) is fulfilled to an accuracy of 10^{-10}.

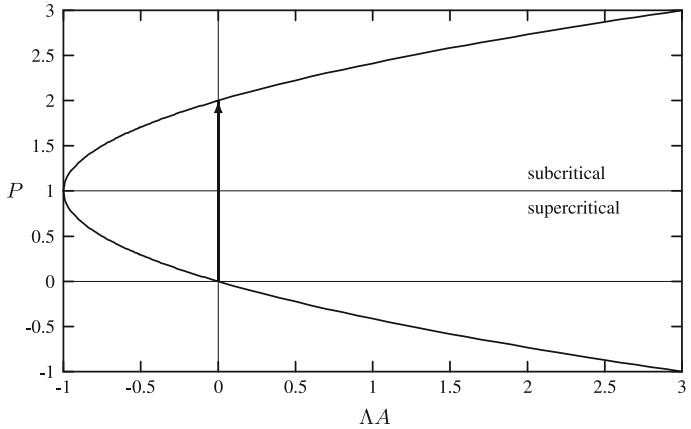

Fig. 6 Pressure-displacement relationship (83) for supercritical upstream conditions. Supercritical and subcritical branches can be connected by a jump discontinuity satisfying hydraulic theory

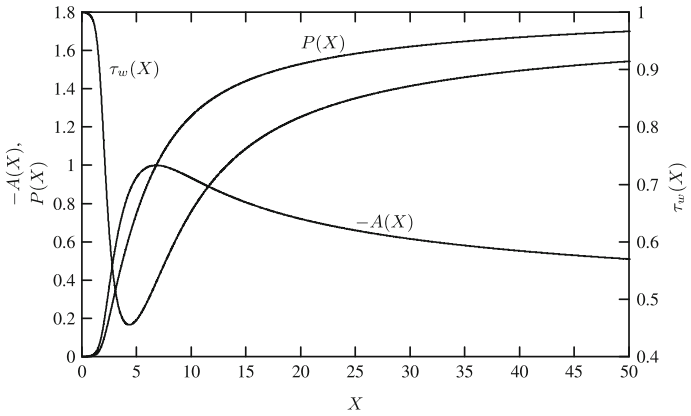

Fig. 7 Structure of hydraulic jump for $W = 0$, $\Lambda = 1$

To initiate the solution, a small pressure disturbance is prescribed at $X = X_i$. An initial profile for U, valid for large negative X is provided by the asymptotic analysis summarized in Sect. 4.1.

Where separated flow is encountered the FLARE approximation, Reyhner and Flügge-Lotz [31] has been adopted which yields reasonably good results for the displayed quantities, in particular for the pressure disturbance and for the displacement thickness, as long as the region of reversed flow remains small, as it is the case for the results presented below.

Two representative examples of eigensolutions in non-dispersive flows $W = 0$ are considered in Figs. 7 and 8 which display the distributions of A, P and the wall shear $\tau_w = \partial U/\partial Y(X, 0)$ for $\Lambda = 1$ and $\Lambda = 0.47$. To initiate the solution, a small positive pressure kick $P = 10^{-4}$ was imposed at $X = 0$. With increasing distance X the pressure is found to rise monotonically which in turn leads to an increase of the perturbation displacement thickness $-A$ and a reduction of the wall shear τ_w. Eventually, the critical state $P = 1$ is reached. Further downstream the perturbation displacement thickness decreases, thus generating a 'viscous' hump with profile $-A(X)$ which triggers the transition from supercritical to subcritical flow conditions. Consequently P continues to rise and approaches the correct downstream value $P = 2$ associated with the prescribed upstream value $P = 0$ asymptotically in the limit $X \to \infty$, see Fig. 6. Owing to the very slow pressure increase for X large, the wall shear increases also and returns to its unperturbed level $\tau_w = 1$.

We also note that the pressure distribution $P(X)$ characterizes the shape of the free surface, and Fig. 7 then describes a structured hydraulic jump from a supercritical flow upstream to subcritical flow downstream.

Inspection of Fig. 8 shows that the flow properties remain unchanged qualitatively if the forcing parameter Λ is reduced to a value of 0.47. According to the definition (50) of Λ and the relationship (17) this reduction of the forcing parameter corresponds to an increase of the Froude number upstream of the bore if the Reynolds number is kept fixed. Consequently, a substantially larger pressure increase is required to achieve the transition

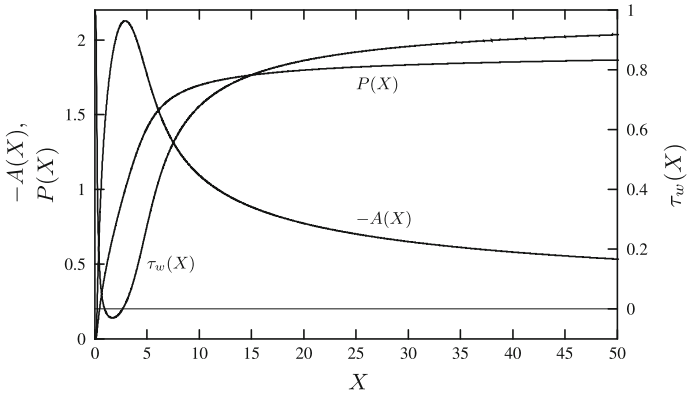

Fig. 8 Structure of hydraulic jumps for $W = 0$, $\Lambda = 0.47$ with the formation of a separated flow region

through the critical state. This phenomenon is not visible in the graph of the (transformed) pressure P which, as before, rises from $P = 0$ to $P = 2$ but has a substantial effect on the distributions of $-A$ and τ_w. Owing to the much larger unfavourable pressure gradient, the viscous wall layer exhibits a significantly larger displacement effect than before, which in turn causes the formation of a separated flow region. Similar to Fig. 7 the minimum of the wall shear occurs well ahead of the maximum of $-A$. The solution of (76) for $W = 0$,

$$\kappa = \kappa_0 = \left(\frac{2}{C\Lambda}\right)^3, \tag{86}$$

shows that a reduction of Λ results in a faster pressure rise initially. This is in agreement with the numerical results depicted in Figs. 7 and 8.

Before turning to a discussion of numerical solutions for dispersive flows it is useful to investigate the properties of eigensolutions far downstream ($X \to \infty$). These have been investigated in [9], extending the work of [33,35].

To study the flow behavior far downstream $X \to \infty$ of a bore it is convenient to introduce the streamfunction $\Psi(X, Y) : U = \partial\Psi/\partial Y$, $V = -\partial\Psi/\partial X$. The expansion of Ψ for $Y \to \infty$ is of the form

$$\Psi(X, Y \to \infty) \sim \frac{1}{2}(Y + A(X))^2 + P(X) + o(Y^{-r}), \quad \forall r. \tag{87}$$

Since the pressure downstream of a bore is known to approach the value $P = 2$ as $X \to \infty$, one obtains the asymptotic behavior

$$\Psi(X \to \infty, Y \to \infty) \sim \frac{1}{2}Y^2 + A(X)Y + 2, \tag{88}$$

which has to be compared with the similarity form of the streamfunction, see [9],

$$\Psi(X \to \infty, Y) \sim \frac{1}{2}Y^2 + CX^\lambda R(\eta) + \cdots, \quad \eta = \frac{Y}{X^{1/3}}, \tag{89}$$

where the eigensolution with eigenvalue λ has the asymptotic behavior

$$R(\eta \to \infty) \sim K_1\eta + K_2\eta^{3\lambda} + K_3 e^{-3\lambda-4} e^{-\eta^3/9}, \quad \lambda \neq \frac{1}{3}. \tag{90}$$

Here K_1 and K_3 are arbitrary constants, while

$$K_2 = \frac{\Gamma(\frac{2}{3})3^{-2\lambda+1/3}}{(3\lambda - 1)\Gamma(\lambda + 1)}. \tag{91}$$

Ψ then in the limit $X \to \infty$, $Y \to \infty$ is given by

$$\Psi(X \to \infty, Y \to \infty) \sim \frac{1}{2}Y^2 + CK_1X^{\lambda-1/3}Y + CK_2Y^{3\lambda}\cdots \tag{92}$$

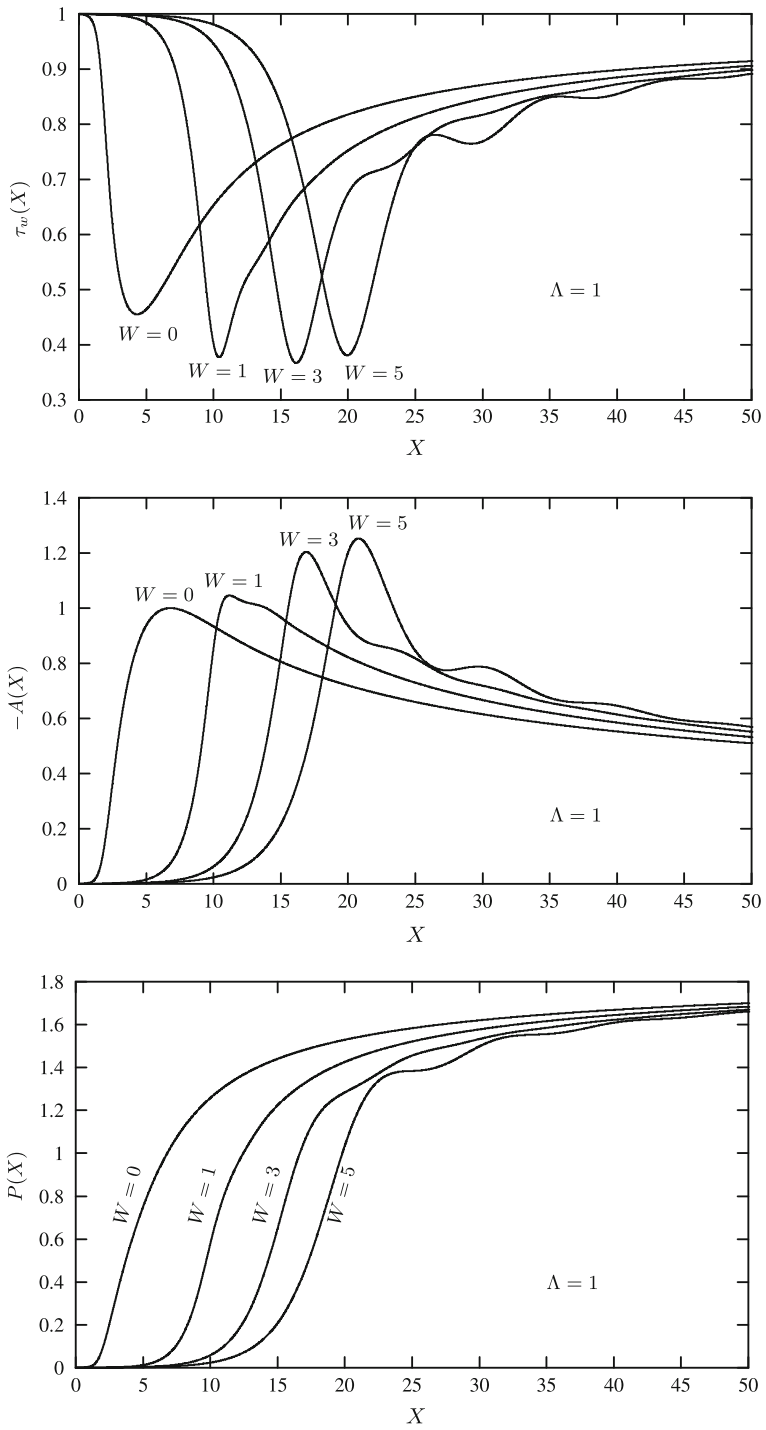

Fig. 9 Effect of the parameter W on the structure of hydraulic jumps for $\Lambda = 1$

From a comparison of Eqs. (88) and (92) one infers that $\lambda = 0$ and

$$A(X \to \infty) \sim \bar{C} X^{-1/3}, \quad \bar{C} = C K_1. \tag{93}$$

Finally, substituting Eq. (93) into the linearized non-dispersive interaction equation yields for the asymptotic behavior of the pressure distribution

$$P(X \to \infty) \sim 2 + \frac{\Lambda \bar{C}}{2} X^{-1/3}. \tag{94}$$

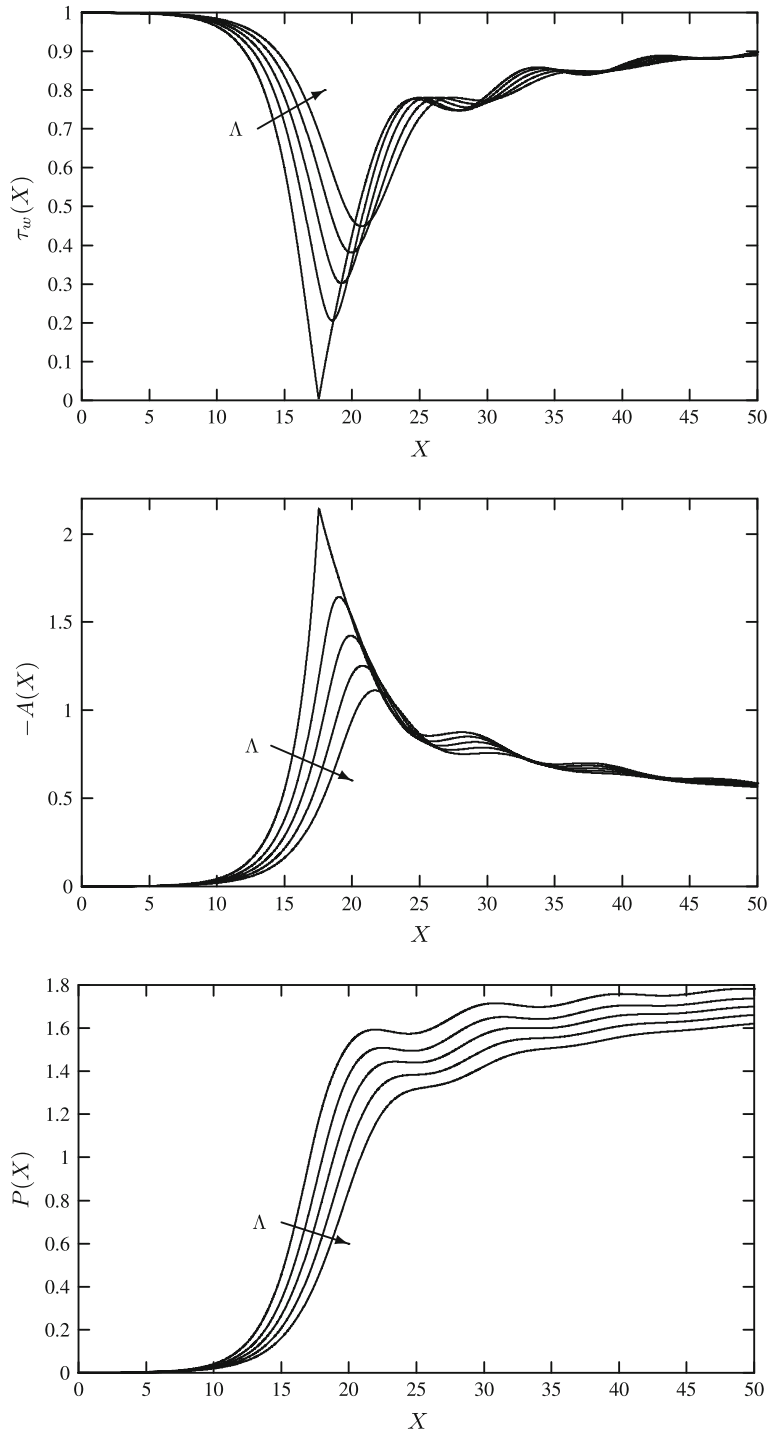

Fig. 10 Effect of the detuning parameter Λ on the structure of hydraulic jumps for $W = 5$ with $\Lambda = (0.674, 0.8, 0.9, 1, 1.1)$

We now turn to a discussion of numerical results for dispersive flows $W > 0$ where the effects caused by streamline curvature dominate the effect of surface tension. In Fig. 9 solutions are presented for Λ fixed and varying W. For $W \ll 1$ an approximate solution of the dispersion relation (76) gives

$$\kappa \sim \kappa_0 - W\kappa_1, \quad \kappa_1 = \frac{3}{2}\kappa_0^3. \tag{95}$$

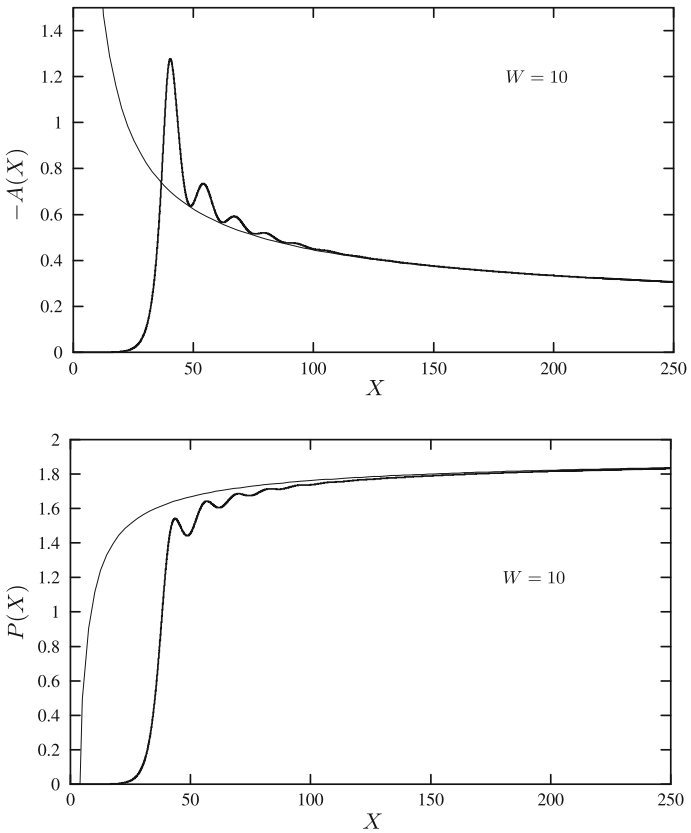

Fig. 11 Comparison of the numerical results for $W = 10$, $\Lambda = 1$ with the asymptotic results (93), (94) for $X \to \infty$

With the upstream behavior given by $P \sim a_1 e^{\kappa x}$, the increasing values of W will delay the initial pressure rise associated with the bore formation. This delay is evident in Fig. 9.

Further downstream, however, the pressure is found to rise faster than in the case of non-dispersive flow which is associated with a reduction of the minimum wall shear. Finally, as to be expected, the pressure rise ceases to be monotonic if the magnitude of the dispersion coefficient is sufficiently large. The resulting pressure oscillations cause the wall shear to oscillate also.

Variations of Λ with $W = 5$ kept fixed are investigated in Fig. 10. As predicted by the dispersion relation (76) decreasing values of Λ result in a faster pressure rise initially but the pressure distribution remains qualitatively unchanged. The associated increase of the pressure gradient, however, is seen to cause a severe thickening of the viscous wall layer. This process is accompanied by the emergence of an increasingly pronounced local maximum of the perturbation displacement thickness $-A(X)$ which eventually is transformed into a kink at $X_c \approx 15.6$ as Λ approaches a critical value $\Lambda \approx 0.674$. Also the wall shear distribution changes drastically in the limit $\Lambda \to \Lambda_c$ where $\tau_w(X)$ exhibits a kink at $X = X_c$ too and $\tau_w(X_c) = 0$. Numerical computations for $\Lambda < \Lambda_c$ point to the occurrence of a singularity upstream of X_c beyond which the solution cannot be continued. The reasons for this breakdown of the interaction equations are not fully understood at present. It should be noted, however, that results similar to those for $\Lambda \approx \Lambda_c$ shown in Fig. 10 have been obtained in the different context of marginally separating laminar boundary layers with imposed rather than induced pressure gradient by [32] and [39]. This suggests that the interaction mechanism envisaged here may be too weak as $X \to X_c$ and has to be modified at least locally, but this has to be investigated yet.

A comparison between numerical results and the asymptotic expressions (93), (94) for $X \to \infty$ is shown in Fig. 11. It is observed that these expressions are well capable of predicting both the rather fast approach of P towards the limiting value 2 and the slow return of A to its upstream value 0.

The flow behavior changes drastically if the effects of surface tension are larger than those caused by streamline curvature, i.e. if $W < 0$, Fig. 12. Even very small negative values of W destroy the exponential pressure rise for $X \to -\infty$ observed if $W > 0$ and result in an oscillatory upstream behavior, again in

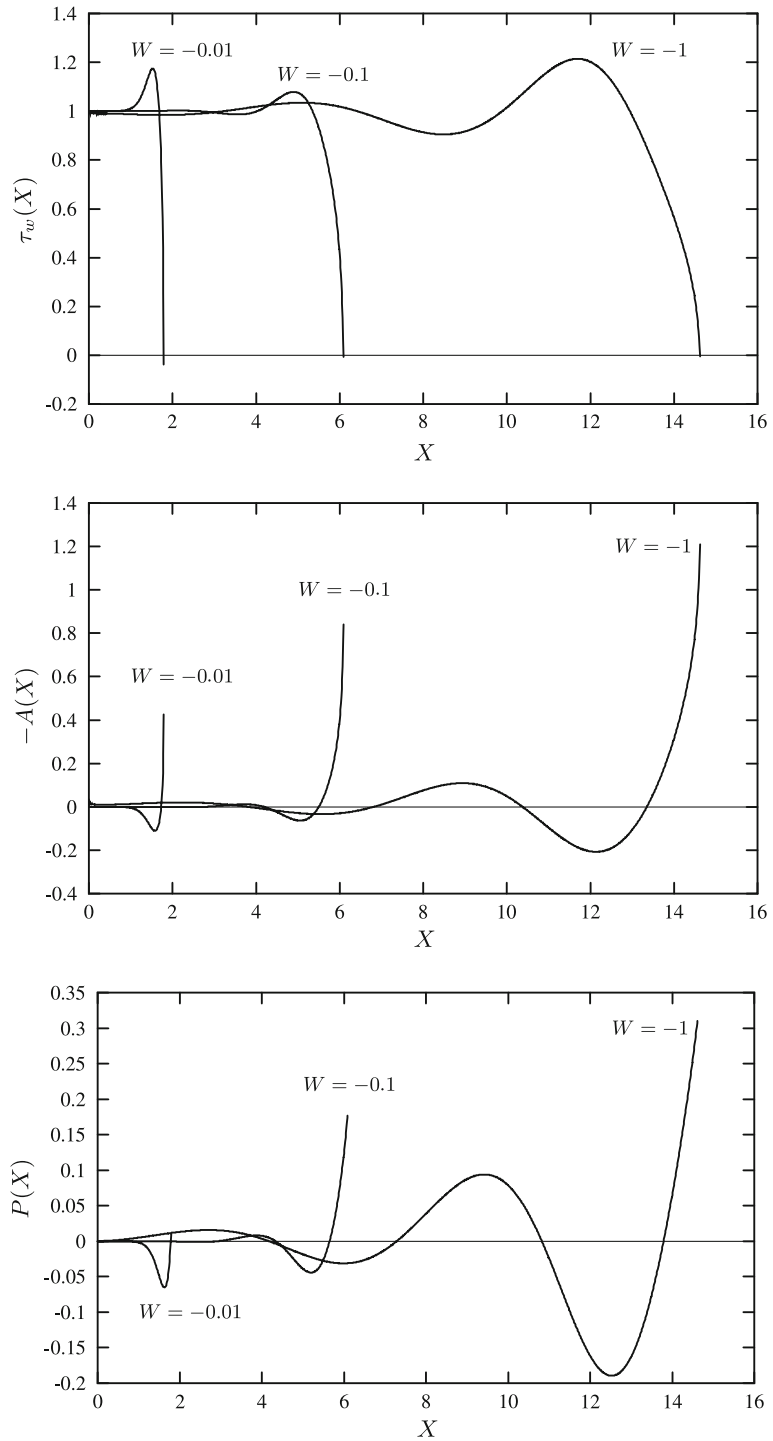

Fig. 12 Numerical results for three cases of negative dispersion and $\Lambda = 1$

agreement with the conclusions based on the structure (84). More importantly, however, there is no tendency towards a pressure plateau as the distance X increases and the numerical scheme eventually ceases to converge due to the occurrence of very large pressure gradients. A similar behavior has been reported in the study by [8] dealing with fully developed flows and it may be related to the formation of a region of reversed flow near the free surface [11]. However, no definite conclusion can be drawn yet.

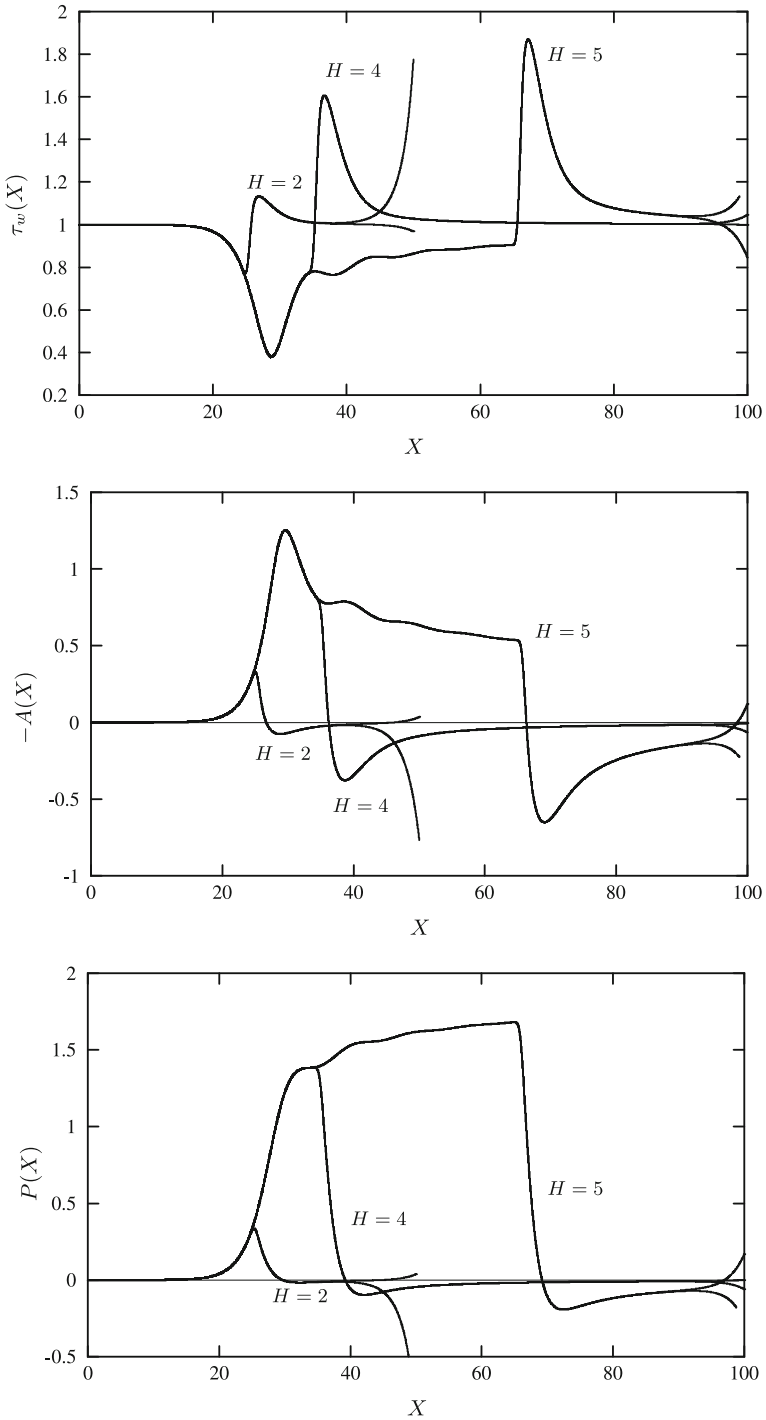

Fig. 13 Interaction of a hydraulic jump with an isolated obstacle of the form (96) for $W = 5$, $\Lambda = 1$ and three values of the parameter H characterizing the height of the obstacle. The observed downstream branching represents the bracketing of the solutions by applying two slightly different upstream initial conditions in the numerical shooting technique

4.3 Interaction of a bore with a surface-mounted obstacle

In the preceding section we have considered (nonlinear) eigensolutions of the lower deck problem (44) to (49) which represent the dissipative-dispersive internal structure of bores. As an example of a nonlinear forced

solution of this problem, Fig. 13 shows numerical results for steady flow past a single hump

$$F(X) = H\mathrm{e}^{-4(X-X_0)^2}. \tag{96}$$

As before, the unperturbed flow is taken to be supercritical. Upstream of the hump where $F = 0$ (essentially) the pressure distribution is given by the eigensolution discussed before. The effect of increasing height H of the obstacle is to push the initial pressure rise associated with this eigensolution further upstream. This is taken into account in Fig. 13 by shifting the obstacle downstream so that the upstream pressure distributions coincide. For small H the flow remains supercritical throughout: $P < 1$ for $-\infty < X < \infty$ and the numerical results are found to agree very well with the predictions (93) and (94) resulting from the linearized version of the fundamental problem. However, if H is sufficiently large, a fully developed bore forms before the hump as can be seen from the result for $H = 5$. This means that the hump now is exposed to a subcritical flow $P > 1$ and, therefore, triggers a transition to supercritical conditions $P < 1$ and, eventually, a return to the unperturbed upstream state $P = 0$. It is interesting to note that this process is associated with an over-expansion of the flow, i.e. the pressure drops too low and slowly recovers.

5 Conclusions

Weakly nonlinear gravity waves in single layer fluids have been studied in the limit of large Reynolds number assuming that viscous effects are confined to a thin boundary layer adjacent to the solid boundary. Asymptotic analysis for $Fr - 1 \to 0$ and $Re \to \infty$ shows that the wave motion in this limit is governed by the classical triple-deck equations. These equations are supplemented, however, with a novel nonlinear interaction law that resembles the evolution equation for small amplitude disturbances in inviscid hydraulic flows and, therefore, allows for the passage through the critical state. Most importantly, it is found that the resulting lower deck problem possesses eigensolutions which describe the viscous dissipative structure of bores.

Numerical solutions of the lower deck problem have been obtained for situations where the (dispersive) effects of streamline curvature dominate over those due to surface tension and vice versa. In the first case eigensolutions are seen to exist for all values of the relevant parameter $W > 0$. For moderately large values of W such solutions can be obtained in a wide range of the detuning parameter Λ being proportional to the inverse of the difference between the unperturbed Froude number and its critical value 1. With increasing detuning, i.e. by decreasing Λ, the minimum of the wall shear stress drops and a separated flow region is formed eventually. Solutions for larger values of W show a different behavior. As before, decreasing values of Λ lead to a reduction of the minimum of the wall shear stress distribution which, however, now is found to exhibit a kink at the point of incipient separation similar to the case of marginally separating boundary layers. Solutions of the interaction problem for smaller values of Λ do not seem to exist, possibly indicating that the interaction mechanism considered here then is too weak and has to be modified at least locally.

While the disturbances of the flow decay exponentially far upstream if $W > 0$ or $W < 0$ and $|W|$ sufficiently small, oscillatory flow behavior is observed for larger values of $|W|$, $W < 0$. As in [2] disturbances of this latter type cannot be marched forward to arbitrary large downstream distances and physically sensible eigensolutions, therefore, cannot be constructed in this case. A somewhat similar difficulty was encountered also by [11] who speculated that it may be associated with the formation of a roller at the free surface.

References

1. Byatt-Smith, J.G.B.: The effects of laminar viscosity on the solution of the undular bore. J. Fluid Mech. **48**, 33–40 (1971)
2. Bowles, R.I., Smith, F.T.: The standing hydraulic jump: theory, computations and comparisons with experiments. J. Fluid Mech. **242**, 145–168 (1992)
3. Bowles, R.I.: Upstream influence and the form of standing hydraulic jumps in liquid-layer flows on favourable slopes. J. Fluid Mech. **284**, 63–96 (1995)
4. Brilliant, H.M., Adamson, T.C.: Shock wave boundary layer interactions in laminar transonic flow. AIAA paper, No. 73-239 (1973)
5. Chester, W.: Resonant oscillations of water waves I. Theory. Proc. Roy. Soc. A **306**, 5–22 (1968)
6. Craik, A., Latham, R., Fawkes, M., Gribbon, P.: The circular hydraulic jump. J. Fluid Mech. **112**, 347–362 (1981)
7. Dutykh, D., Dias, F.: Viscous potential free-surface in a fluid layer of finite depth. C.R. Acad. Sci. Paris, Ser. I **345**, 113–118 (2007)
8. Gajjar, J., Smith, F.T.: On hypersonic self-induced separation, hydraulic jumps and boundary layers with algebraic growth. Mathematika **30**, 77–93 (1983)

9. Gittler, P.H.: On similarity solutions occurring in the theory of interactive laminar boundary layers. J. Fluid Mech. **244**, 131–147 (1992)
10. Grimshaw, R.H.J., Smyth, N.F.: Resonant flow of a stratisfied fluid over topography. J. Fluid Mech. **169**, 429–464 (1986)
11. Higuera, F.: The hydraulic jump in a viscous laminar flow. J. Fluid Mech. **274**, 69–92 (1994)
12. Johnson, R.S.: Shallow water waves on a viscous fluid – the undular bore. Phys. Fluids **15**, 1693–1699 (1972)
13. Johnson, R.S.: A modern introduction to the mathematical theory of water waves. Cambridge University Press, Cambridge (1997)
14. Kakutani, T., Matsuuchi, K.: Effect of viscosity on long gravity waves. J. Phys. Soc. Jpn. **39**, 237–246 (1975)
15. Kluwick, A.: Small amplitude finite-rate waves in fluids having positive and negative nonlinearity. In: Kluwick, A. (ed.) Nonlinear Waves in Real Fluids. CISM Courses and Lectures No. 315, pp. 1–43. Springer, New York (1991)
16. Kluwick, A.: Interacting laminar and turbulent boundary layers. In: Kluwick, A. (ed.) Recent Advances in Boundary Layer Theory. CISM Courses and Lectures No. 390, pp. 231–330. Springer, New York (1998)
17. Kluwick, A., Gittler, Ph.: Transonic laminar interacting boundary layers in narrow channels. ZAMM **81**, 473–474 (2001)
18. Lamb, H.: Hydrodynamics. Cambridge University Press, Cambridge (1932)
19. Larras, M.: Ressaut circulaire sur fond parfaitement lisse. C.R. Adac. Sci. Paris **225**, 837–839 (1962)
20. Lighthill, M.J.: On boundary layers and upstream influence II. Supersonic flows without separation. Proc. Roy. Soc. A **217**, 478–504 (1953)
21. Lighthill, M.J.: Waves in Fluids. Cambridge University Press, Cambridge (1978)
22. Liu, P.L., Orfila, A.: Viscous effects on transient long-wave propagation. J. Fluid Mech. **520**, 83–92 (2004)
23. Liu, P.L., Park, Y.S., Cowen, E.A.: Boundary layer flow and bed shear stress under a solitary wave. J. Fluid Mech. **574**, 449–463 (2007)
24. Mei, C.C., Liu, P.L.: The damping of surface gravity waves in a bounded liquid. J. Fluid Mech. **59**, 239–256 (1973)
25. Miles, J.W.: Korteweg-de Vries equation modified by viscosity. Phys. Fluids **19**, 1063 (1976)
26. Nakoryakov, V.E., Pokusaev, B.G., Troyan, E.N.: Impingement of an axisymmetric liquid jet on a barrier. Int. J. Heat Mass Transfer **21**, 1175–1184 (1978)
27. Oldham, K.B., Spanier, J.: The fractional calculus. Academic Press, New York (1974)
28. Olson, R.G., Turkdogan, E.T.: Radial spread of a liquid stream on a horizontal plate. Nature **211**, 813–816 (1966)
29. Peregrine, D.H.: Surface shear waves. J. Hydrol. Div. ASCE **100**, 1215–1227 (1974)
30. Rayleigh, L.: On the theory of long waves and bores. Proc. Roy. Soc. A **90**, 324–328 (1914)
31. Reyhner, T.A., Flügge-Lotz, I.: The interaction of a shock wave with a laminar boundary layer. Int. J. Nonlinear Mech. **3**, 173–199 (1968)
32. Ruban, A.I.: Singular solution of boundary layer equations which can be extended continuously through the point of zero surface friction. Izv. Akad. Nauk SSSR, Mekh. Zhidk. Gaza **6**, 42–52 (1981)
33. Smith, F.T.: The laminar separation of an incompressible fluid streaming past a smooth surface. Proc. Roy. Soc. A **356**, 433–463 (1977)
34. Smith, F.T.: On the high Reynolds number theory of laminar flows. IMA J. of Appl. Maths **28**, 207–281 (1982)
35. Smith, F.T., Merkin, J.H.: Triple-deck solutions for subsonic flow past humps, steps, concave or convex corners and wedged trailing edges. Comput. Fluids **10**, 7–25 (1982)
36. Stewartson, K.: Multistructured boundary layers on flat plates and related bodies. Adv. Appl. Mech. **14**, 145–239 (1974)
37. Smyth, N.F.: Modulation theory for resonant flow over topography. Proc. Roy. Soc. A **409**, 79–97 (1987)
38. Stewartson, K., Williams, P.G.: Self-induced separation. Proc. Roy. Soc. A **312**, 181–206 (1969)
39. Stewartson, K., Smith, F.T., Kaups, K.: Marginal separation. Stud. Appl. Math. **67**, 45–61 (1982)
40. Sugimoto, N.: Generalized Burgers equation and fractional calculus. In: Jeffrey, A. (ed.) Nonlinear Waves Motion, pp. 162–179. Longman, New York (1989)
41. Watson, E.J.: The radial spread of a liquid jet over a horizontal plane. J. Fluid Mech. **20**, 481–499 (1964)
42. Whitham, G.B.: Linear and Nonlinear Waves. Wiley, New York (1974)